

Electron and photon energy deposition in the UniverseToru Kanzaki¹ and Masahiro Kawasaki^{1,2}¹*Institute for Cosmic Ray Research, University of Tokyo, Kashiwa 277-8582, Japan*²*Institute for the Physics and Mathematics of the Universe, University of Tokyo, Kashiwa 277-8582, Japan*

(Received 8 July 2008; published 6 November 2008)

We consider energy deposition of high energy electrons and photons in the Universe. We carry out detailed calculations of fractions of the initial energy of the injected electron or photon which are used to heat, ionize, and excite background plasma in the early Universe for various ionization states (ionization fraction = $10^{-3} - 1$) and redshifts ($z = 100-1000$).

DOI: 10.1103/PhysRevD.78.103004

PACS numbers: 95.30.Jx

I. INTRODUCTION

The energy deposition of fast electrons and high energy photons in partly ionized plasma is an important issue in the wide range of physics and astrophysics. In cosmology, for example, the high energy photons and/or electrons are injected from decay or annihilation of massive particles. The recent observation of the Wilkinson Microwave Anisotropy Probe (WMAP) on the cosmic microwave background (CMB) has shown that dark matter constitutes about 80% of the total matter in the Universe [1]. One of the most promising candidates for dark matter is a supersymmetric particle with mass $O(100)$ GeV. If such massive particles are annihilated and/or decay, the ejected charged particles and photons interact with various background particles—the electron, atomic hydrogen, and the CMB photon—and hence give the significant effects on the thermal history of the Universe. In this case, to estimate the cosmological effect of dark matter annihilation/decay precisely, we need to understand development of electromagnetic cascade showers induced by primary particles, energy loss of charged particles and photons, and so on. Besides dark matter, there are many candidates for inducing electromagnetic showers and affecting the cosmic background plasma in physics beyond the standard model.

When the high energy electrons and photons are emitted before recombination, they may change abundances of light elements produced in the big bang nucleosynthesis and/or may distort the CMB spectrum, which has been extensively studied (e.g., see references for big bang nucleosynthesis in [2] and for the CMB in [3]). On the other hand, if the high energy photons and electrons are injected after recombination, they can cause ionization and excitation of neutral hydrogens as well as scatterings off background photons and free electrons. Thus, the thermal history of the Universe, in particular, ionization fraction and electron temperature, may significantly change compared with the standard case, and it gives the change of the temperature and polarization angular power spectra measured precisely by the WMAP. To estimate the influence on CMB anisotropies, detailed calculations for electron/photon energy deposition is necessary. The energetic electrons

lose their energy by inverse Compton scattering which is very fast because of the huge number density of the CMB photons. For high energy photons, their interaction rate with the background electrons and hydrogen is not as fast as photon-photon processes, and the typical rate of Thomson scattering is given by $t_{pe} \approx 2 \times 10^{20}(1+z)^{-3}$ sec. Therefore, the interaction time of the high energy photons and electrons is much faster than the cosmic expansion for $z \geq 100$. Since neglect of the cosmic expansion largely simplifies the present analysis, we consider the range of redshift between 100 and 1000.

Detailed calculations for electrons and photons slowing down in partially ionized plasma of atomic hydrogen were carried out by many authors (see references in [4]). However, these authors mainly studied the case of injected electron energy up to keV. On the other hand, when dark matter annihilation/decay takes place, the high energy photons and electrons with energy $O(1)$ are produced, and the previous calculations are not enough at all for studying its effect on the CMB angular power spectra. Although some authors investigated this subject [5,6], they extrapolated carelessly the result of energy deposition of electrons/photons which is valid up to keV. In this paper, therefore we extended the previous calculations which are valid up to a much higher energy, i.e., 1 TeV. The injected high energy particles produce the cascade showers and lose their energy. We can categorize three types of energy loss: *heat*, *excitation*, and *ionization* according to what the energy of the particle is used for. It is the aim of this paper to derive these quantities precisely. They depend on the energy of primary particles as well as the redshift and state of ionization. There are two reasons why it is difficult to derive them. One is the large number of interactions involved with the energy degradation. The other is the connection between the energy degradation of charged particles and that of photons. For example, high energy electrons can produce photons as much the same energy through inverse Compton scatterings with CMB photons. In other words, we cannot calculate the evolution of the energy of charged particles and photons separately but simultaneously.

In Sec. II, we show the numerical method to calculate the energy degradation of the primary particles. In Sec. III, the evolutions of the energy of the primary electron, photon, and positron are presented. The results of the energy degradation of the primary particles is shown in Sec. IV. In Sec. V, we summarize the results.

II. NUMERICAL METHOD

For incident electrons and photons, there are many interactions which contribute to energy degradation. It is convenient to divide these processes into two groups. One is the group characterized by losing only a very small portion of energy in one collision (continuous loss). The other is the group characterized by being likely to lose a significant portion of energy in one collision (“catastrophic” loss [7]). In the case of the latter, it is necessary to use an integro-differential equation to calculate the electron energy spectrum.

Let E_1, E_2, \dots, E_N be a discrete set of energies of particles ($E_i < E_j$ for $i < j$) and $N_p(E_s)\Delta E_s$ be the number of particles with energy between $E_s - \Delta E_s/2$ and $E_s + \Delta E_s/2$. The accuracy of the numerical method is limited by the bin size (ΔE_i). Since we consider very large energy region ranges from 10 eV to 100 GeV, the bin sizes are taken to increase as energy so that $\Delta E_i/E_i$ become constant. The particle energy spectrum is given by

$$\frac{\partial N_p(E_s)}{\partial t} = -\frac{1}{\Delta E_s} \left[\frac{-dE}{dt} \right] N_p(E_s) - N_p(E_s) \sum_{i < s} P(E_s, E_i) + \sum_{i > s} N_p(E_i) P(E_i, E_s) + Q(E_s), \quad (1)$$

where $P(E_i, E_j)dt$ is the probability that a particle with energy E_i undergoes a collision, causing it to lose energy and have energy E_j in time dt , and $Q(E_i)$ represents sources and sinks of particles corresponding to the possible production, annihilation, or gradual leakage from the energy range that we consider [8]. The first term of the right-hand side of Eq. (1) represents continuous loss, and the second and third terms represent outflow and inflow, respectively, caused by catastrophic loss.

In this paper, we are mainly interested in how much initial particle energy converts to heat, excitation, and ionization. For convenience, we define $\chi_h(E)$, $\chi_e(E)$, and $\chi_i(E)$ as fractions of the initial energy E which go to heat, excitation, and ionization, respectively. They are written as

$$\chi_i = \frac{E_{1f}}{E} \langle N_i \rangle, \quad (2)$$

$$\chi_e = \frac{1}{E} \sum_j E_{1j} \langle N_{1s \rightarrow j} \rangle, \quad (3)$$

$$\chi_h = 1 - \chi_i - \chi_e, \quad (4)$$

where E_{1f} is ionization energy and E_{1j} is the energy

difference between the ground state and the j th excited state. The average numbers of ionization and excitations through radiative processes are represented as $\langle N_i \rangle$ and $\langle N_{1s \rightarrow j} \rangle$, respectively. Note that $\chi_i + \chi_e + \chi_h = 1$.¹ Here, for simplicity, we assume that all baryons in the Universe are free protons and hydrogen atoms and neglect helium, which causes at most a 10% error in our calculation.

Suppose that we know already $\chi_h(E_i)$, $\chi_e(E_i)$, and $\chi_i(E_i)$ with energy less than E_s , and consider a particle with initial energy E_s . Since there are no particles with energy more than E_s , the energy degradation is characterized by the first term of the right-hand side of Eq. (1) (continuous loss), the second term (catastrophic loss), and the last term (annihilation). Here we consider only that annihilation of the primary particle contributes to $Q(E_s)$. All of these terms are in proportion to $N_p(E_s)$, so we define the following number loss function:

$$L(E_s) = \frac{1}{\Delta E_s} \left[\frac{-dE}{dt} \right] + \sum_i n_t v_p \sigma_i(E_s), \quad (5)$$

where n_t is the number density of target particle, v_p is the particle velocity, and $\sigma_i(E_s)$ is the catastrophic and annihilation cross sections. From the number loss function, we can obtain the probability that a particle undergoes a particular collision “ m ” [9]. The collision frequency for a particular continuous loss may be defined by

$$\nu_m(E_s, E_{s-1}) = \frac{1}{\Delta E_s} \left[\frac{-dE}{dt} \right]_m, \quad (6)$$

and the collision frequency for a particular catastrophic loss “ α ” and annihilation “ β ” are given by

$$\nu_\alpha(E_s, E_i) = n_t v_p \sigma_\alpha(E_s, E_i), \quad (7)$$

and

$$\nu_\beta(E_s) = n_t v_p \sigma_\beta(E_s), \quad (8)$$

respectively. The total collision frequency for the catastrophic loss is given by

$$\nu_\alpha(E_s) = \int dE n_t v_p \sigma_\alpha(E_s, E). \quad (9)$$

Then the probability $P(E_s, E_i)$ is written as

$$P(E_s, E_i) = \frac{\sum_\alpha \nu_\alpha(E_s, E_i)}{\sum_m \nu_m(E_s, E_{s-1}) + \sum_\alpha (\nu_\alpha(E_s) + \nu_\beta(E_s))} \quad (i \neq s-1), \quad (10)$$

¹We frequently use “fraction of heat,” “fraction of excitation,” and “fraction of ionization” to refer to χ_h , χ_e , and χ_i , respectively. Please do not confuse χ_i with “ionization fraction” x_e which is the fraction of ionized hydrogens.

$$P(E_s, E_{s-1}) = \frac{\sum_m \nu_m(E_s, E_{s-1}) + \sum_\alpha \nu_\alpha(E_s, E_{s-1})}{\sum_m \nu_m(E_s, E_{s-1}) + \sum_\alpha (\nu_\alpha(E_s) + \nu_\beta(E_s))}. \quad (11)$$

Combining these probabilities with the data about $\chi_h(E)$, $\chi_e(E)$, and $\chi_i(E)$ with energy less than E_s , $\chi_h(E_s)$, $\chi_e(E_s)$, and $\chi_i(E_s)$ can be obtained. Please notice that the definition of the frequency for continuous loss depends on the size of the energy bin but the final result is independent of it. The reason is as follows. When all of the bins are divided into halves, the probability $P(E_s, E_i)$ decreases by 50% if the bin size is small enough. This is because the collision frequency for continuous loss is much larger than that for catastrophic loss in this case. However, the effect of the decrease of the probability is cancelled by the increase of the bin numbers. We have checked that our results are independent of the size of the energy bin.

III. INDIVIDUAL EVOLUTION

A. Electron

For incident high energy electrons, there are many interactions which contribute to energy degradation: elastic collision with atomic hydrogen, excitation and ionization of atomic hydrogen, Coulomb loss with background electrons, and inverse Compton scattering with background photons (CMB photons). The cross sections and energy loss rates of these interactions are described in the appendix and shown in Figs. 1 and 2. Hereafter, we use electron kinetic energy (K_e) instead of electron energy ($E_e = K_e + m_e$) for convenience. In this paper, we have used a 4 level ($2s$, $2p$, $n = 3$ and $n > 3$) approximation in considering electron impact excitation. From Fig. 1, it is found that energy loss is dominated by collisions with a background electron (Coulomb loss) at low energy and inverse Compton scattering off a CMB photon at high energy. The reason is simple. At low energy, the average energy loss of an electron is roughly $\Delta E_e \propto \beta^2 E_{\text{CMB}}$ for one inverse Compton scattering. So electrons lose a very small fraction of their energy, and hence energy loss is dominated by collisions with atomic hydrogen and background electrons. On the other hand, at high energy, since the number density of a CMB photon is much larger than that of a background electron, energy loss is dominated by inverse Compton scattering. Energy loss by Coulomb collisions is so efficient that free electrons with ionization fraction x_e exceeding 10^{-4} have a substantial influence on the energy degradation [4]. Thus, as the ionization fraction increases, the fraction of the initial electron energy which is converted to heat [$\chi_h(E)$] increases as shown later.

We calculate the energy degradation of an electron following the method described in the previous section. There are two free parameters: ionization fraction x_e and redshift $1 + z$. The ionization fraction is relevant for collisions with atomic hydrogens and background electrons, and the redshift is mostly relevant for inverse Compton

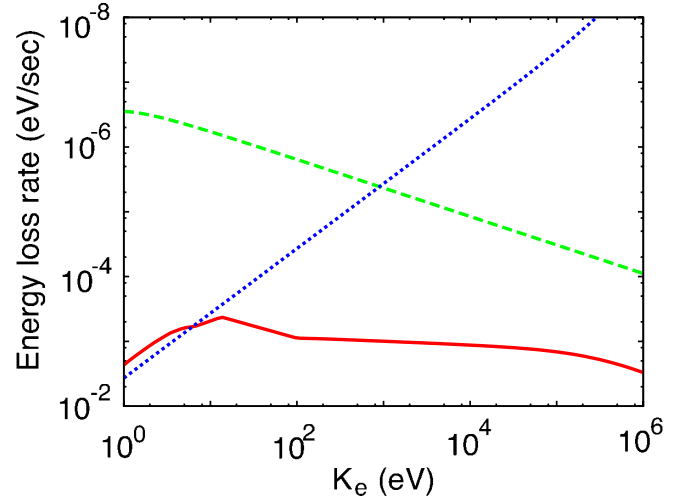


FIG. 1 (color online). Continuous energy loss rates for electrons with $x_e = 10^{-2}$ and $1 + z = 1000$. The solid line represents an elastic collision with atomic hydrogen, the dashed line represents Coulomb loss with a background electron, and the dotted line represents inverse Compton scattering with a CMB photon.

scattering. For simplicity, we regard the distribution of CMB photons as monoenergetic [$E_\gamma = 6.34 \times 10^{-13}(1 + z)$ GeV], not blackbody. Free and bound proton number densities can be parametrized by baryon-to-photon ratio η : $n_p = \eta n_{\text{CMB}}$. We adopt $\eta = 6.1 \times 10^{-10}$ from the result of the WMAP 3-year observation [1]. We take into account properly secondary electrons which are produced by electron impact ionization.

Energy degradation for several values of x_e and $1 + z$ is shown in Figs. 3–5. Here we plot $\chi_h(E)$, $\chi_{\text{ex}}(E)$, and $\chi_i(E)$. In addition, we also plot the fraction of the initial energy that goes to photons with energy larger than $Ry (= 13.6 \text{ eV})$. This energy is the threshold energy for

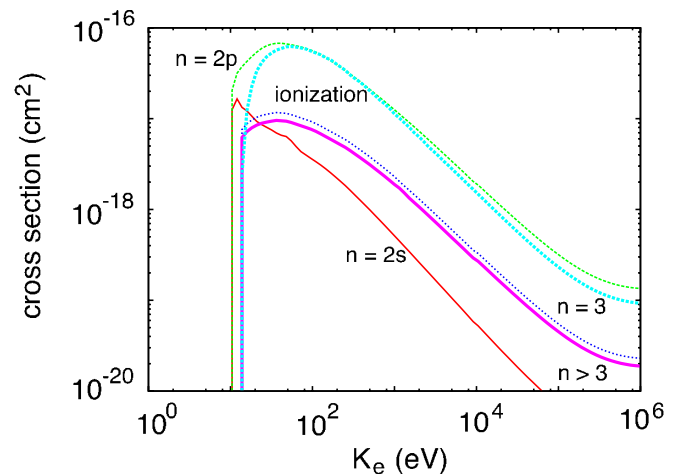


FIG. 2 (color online). Cross sections for electron impact excitation and ionization of H.

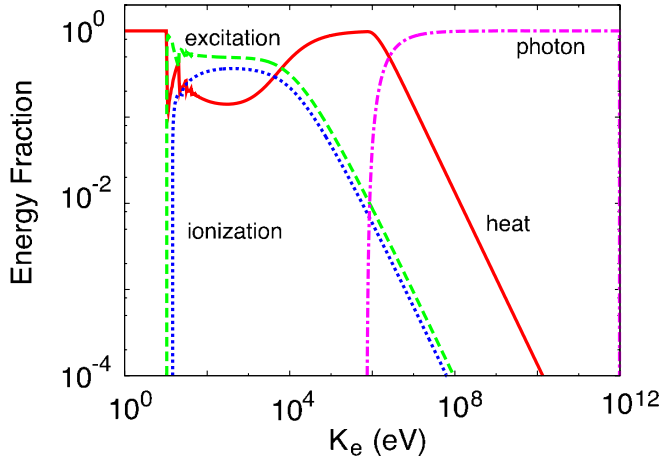


FIG. 3 (color online). Electron energy degradation with $x_e = 0$ and $1 + z = 1000$. The solid line represents χ_h , the dashed line represents χ_{ex} , and the dotted line represents χ_i . The dotted-dashed line represents the fraction of photon energy whose energy is larger than Ry.

photoionization; it is granted that these photons also contribute to heat, excitation, and ionization, and we will treat them in Sec. IV. On the other hand, photons with energy less than Ry heat only background electrons with Compton scattering. An oscillating behavior below 50 eV in Figs. 3 and 5 reflects the nature of discrete energy loss. This behavior is not seen in Fig. 4 since the effect of Coulomb loss dominates over ionization and excitation. The common features in Figs. 3–5 are as follows: (i) The fractions of heat, excitation, and ionization are the same order for $E_e < 10^4$ eV, (ii) heat dominates at $10^4 < E_e < 10^6$ eV, and (iii) finally, the energy of photons dominates for $E_e > 10^7$ eV. At relatively low energy, inverse Compton scat-

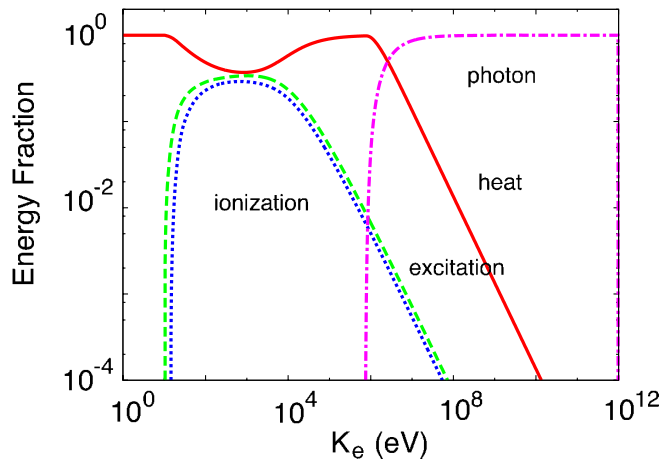


FIG. 4 (color online). Electron energy degradation with $x_e = 10^{-2}$ and $1 + z = 1000$. The solid line represents χ_h , the dashed line represents χ_{ex} , and the dotted line represents χ_i . The dotted-dashed line represents the fraction of photon energy whose energy is larger than Ry.

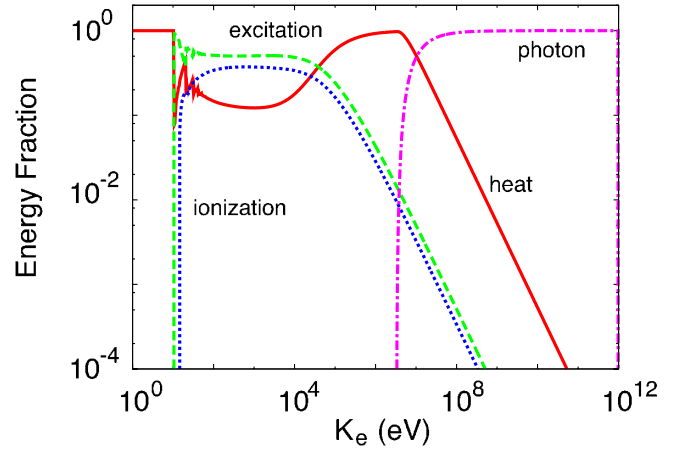


FIG. 5 (color online). Electron energy degradation with $x_e = 0$ and $1 + z = 100$. The solid line represents χ_h , the dashed line represents χ_{ex} , and the dotted line represents χ_i . The dotted-dashed line represents the fraction of photon energy whose energy is larger than Ry.

tering is inefficient. Moreover, the cross sections and energy loss rates for momentum loss, excitation, and ionization are almost the same order if the ionization fraction is not large; i.e., Coulomb loss is not dominant. As a consequence, χ_h , χ_{ex} , and χ_i are nearly the same order, and our calculation corresponds to the result of Ref. [4] up to $E_e \sim \text{keV}$. As electron energy increases, inverse Compton scattering becomes significant. If the energy of a scattered-up photon is less than the threshold energy of photoionization, the energy loss due to inverse Compton scattering converts to heat and the fraction of heat approaches to unity. When electron energy further increases and most of the scattered-up photons have enough energy to ionize atomic hydrogen, the energy of an incident electron exclusively converts to the photon energy.

Next we will show how these fractions are dependent on parameters. To see the effect of the ionization fraction, let us compare Fig. 3 with Fig. 4. It can be seen that the fraction of heat increases at low energy as the ionization fraction increases. This is because Coulomb collision which is proportional to electron density x_e converts initial electron energy into heat exclusively. On the other hand, the collision frequencies for ionization and excitation do not change for $x_e \ll 1$ since they are proportional to the number density of hydrogen atom $(1 - x_e)$. As a result, the fraction of heat increases while the ionization and excitation fractions decrease. At high energy, the results are irrelevant for the ionization fraction since inverse Compton scattering dominates over all other processes. Comparing Fig. 3 with Fig. 5, it can be seen that the rise of heat and photon energy shifts to the high energy side as the redshift decreases. This is because the effect of inverse Compton increases in proportion to the energy of the CMB photon and hence in inverse proportion to the redshift.

B. Photon

As well as the electron, there are many interactions which contribute to energy degradation for incident high energy photons: photoionization, Compton scattering with background electrons, pair production in matter, photon-photon scattering, and double photon pair creation. Here we neglect photoexcitation since the resultant excited state immediately emits a photon and goes down to the ground state. The cross sections and energy loss rates of these interactions are found in the appendix and shown in Fig. 6.

Energy degradation is plotted for $x_e = 0$ and $1 - x_e = 10^{-2}$ in Figs. 7 and 8. Here we plot χ_h and χ_i . In addition, we also plot the fraction of initial energy which goes to electrons with energy larger than 0.75 Ry. This energy is the threshold for electron impact excitation of atomic hydrogen. Electrons with lower energy only heat background electrons through elastic collision with atomic hydrogen and Coulomb loss. The sudden falls of χ_h reflects the nature of discrete energy loss. The energy for the first fall ($E_\gamma = \text{Ry}$) corresponds to the threshold energy of photoionization, and the second one ($E_\gamma = 7/4\text{Ry}$) corresponds to the sum of the threshold energy of photoionization and that of electron impact excitation. In that case, the energy of the incident photon goes into ionization and the electron produced in the ionization and is not used for heating. (Of course, the electron further interacts with background plasma and heats it. This will be taken account in the next section.) The rise of χ_h around $E_\gamma \sim 10^4$ eV is due to Compton scattering. Unlike the case of an incident electron, the fraction of electron energy dominates even at low energy. This is because energetic electrons are produced through photoionization at low energy and Compton scattering at high energy.

The increase of the ionization fraction causes the increases χ_h especially at low energy. This is because photoionization and Compton scattering determine the

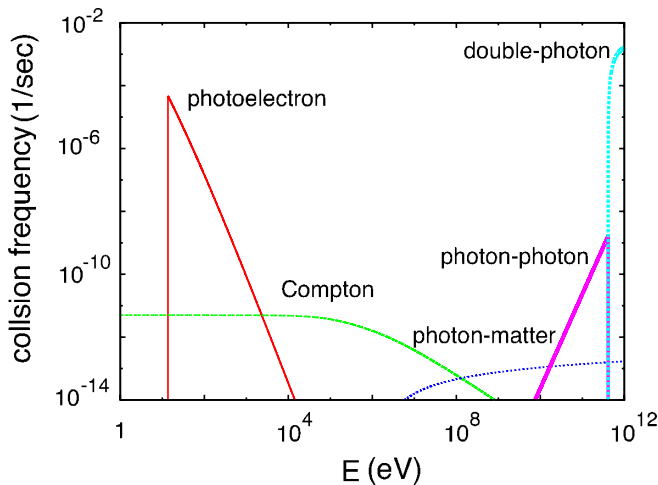


FIG. 6 (color online). Photon collision frequencies with $x_e = 0$ and $1 + z = 1000$.

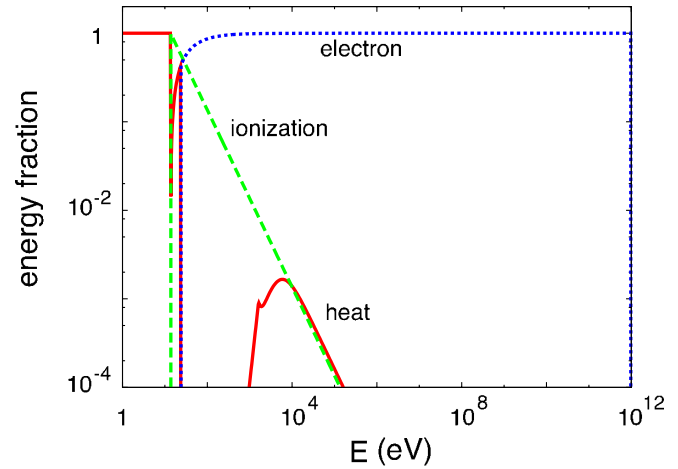


FIG. 7 (color online). Photon energy degradation with $x_e = 0$ and $1 + z = 1000$. The solid line represents χ_h , the dashed line represents χ_i , and the dotted line represents the fraction of electron energy whose energy is larger than 0.75 Ry.

degradation of electron energy at low energy. The effect of photoionization decreases as the ionization fraction increases, and hence χ_h increases. Since the photoionization rate is proportional to $(1 - x_e)$, the effect of photoionization becomes small as x_e approaches 1, which leads to relative enhancement of Compton scattering and increases χ_h . Note that we use the baryon density instead of the electron density when we calculate the energy losses due to Compton scattering. This is because Compton scattering becomes important only when E_γ is sufficiently larger than Ry and the interaction is insensitive to whether an electron is bound or not [5]. As the redshift increases, photon-photon scattering and double photon pair creation become important. These processes, however, become

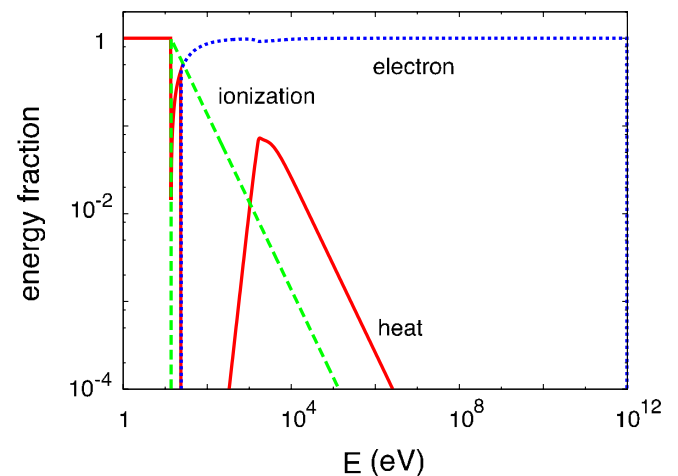


FIG. 8 (color online). Photon energy degradation with $1 - x_e = 10^{-2}$ and $1 + z = 1000$. The solid line represents χ_h , the dashed line represents χ_i , and the dotted line represents the fraction of electron energy whose energy is larger than 0.75 Ry.

dominant at very high energy as seen in Fig. 6. This effect does not appear until the energy deposition of the electron and positron is taken into account.

C. Positron

Positrons are produced by pair production in the electric field of nuclei and double photon pair creation. Therefore, we should take the energy degradation of positrons into account. Although the energy degradation of positrons is almost the same as that of electrons, there are two differences between the electron and the positron. One is the sign of its charge. The other is the indistinguishability between a primary electron and a secondary electron in the processes where the target is an electron or atomic hydrogen. These differences become less important at high energy. For simplicity, we assume positrons lose their energy just like electrons in this paper. Besides, positrons finally annihilate with background electrons through either free annihilation or the formation and decay of positronium [10]. It depends on the temperature, density, and state of ionization of the background electron which process is dominant. Roughly speaking, most of the positrons undergo annihilation after the significant loss of their energy. Therefore, we assume that a positron forms positronium with a background electron after losing almost all of its energy and decay. The positronium annihilates to two photons (each 0.511 MeV) 25% of the time and to three photons (each less than 0.511 MeV) 75% of the time. The energy spectrum from the three-photon annihilation is described in the appendix.

IV. RESULTS

As previously mentioned, we should calculate the evolution of the energy of charged particles and photons simultaneously. In Figs. 3–5 (7 and 8), the fractions of heat, ionization, and excitation are only due to primary and secondary electrons (photons), and the contribution of the secondary photons (electrons) produced in various radiative processes is not included in them. Instead, in the figures, we show the fraction of the initial energy that goes to energetic photons (electrons). For a complete estimation of χ_i , χ_e , and χ_h , we should calculate the contributions of such photons (electrons) to the fraction of heat, ionization, and excitation. In our method, it is easy to calculate it since we already know the spectrum of the secondary particles. In Figs. 9 and 10, we show the fraction of heat, excitation, and ionization when the primary particle is an electron and a photon, respectively. Let us examine these figures.

First, we consider the electron case. When the energy of the electron is small ($K_e < 10^4$ eV) and the ionization fraction is not large, the fractions of heat, excitation, and ionization are roughly the same order. This is because the relative smallness of the ionization fraction makes the effect of Coulomb loss comparable with that of excitation

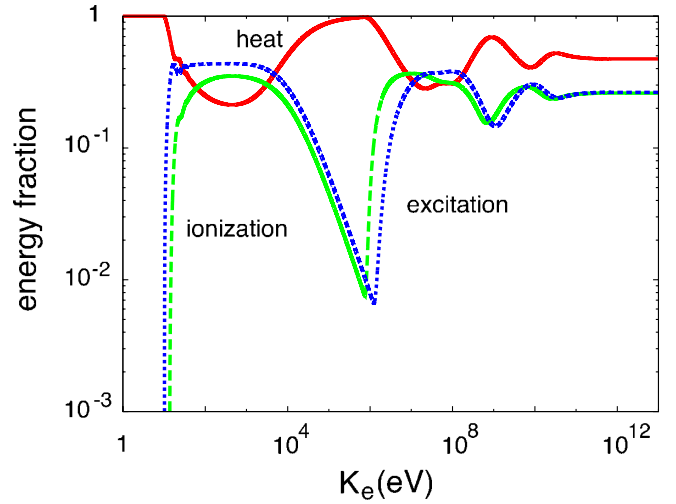


FIG. 9 (color online). Electron energy degradation with $x_e = 10^{-3}$ and $1 + z = 1000$. The solid line represents χ_h , the dashed line represents χ_i , and the dotted line represents χ_{ex} .

and ionization of atomic hydrogen. The fraction of heat increases as the ionization fraction increases and vice versa. For larger electron energy ($K_e > 10^4$ eV), the dominant energy loss mechanism is the inverse Compton scattering. If the electron is nonrelativistic, the energy of scattered-up photons is so small that these photons contribute only to heating of the background particles. As a consequence, the fraction of heat reaches near unity. When an electron is relativistic, the energy of scattered-up photons exceeds the threshold energy of ionization of atomic hydrogen. In this case, it is necessary to estimate the contribution of these photons. It is seen that the fractions of excitation and ionization are a little larger than that of heat with low photon energy in Fig. 10. For this reason, all of these fractions become almost the same amount. The

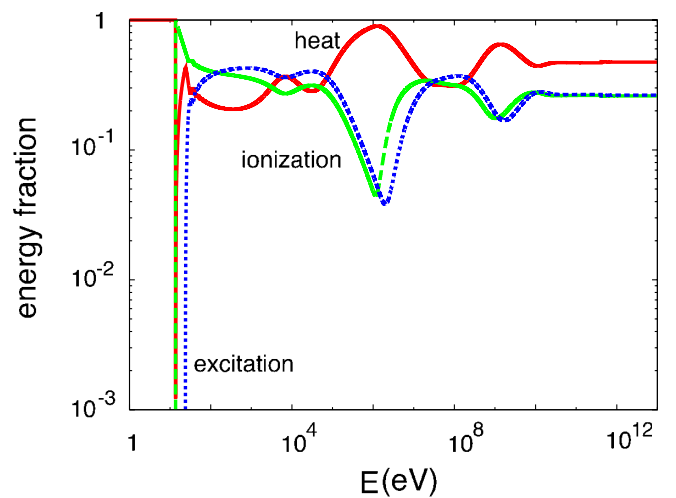


FIG. 10 (color online). Photon energy degradation with $x_e = 10^{-3}$ and $1 + z = 1000$. The solid line represents χ_h , the dashed line represents χ_i , and the dotted line represents χ_{ex} .

oscillating structure of the χ 's around $K_e \approx 10^8$ – 10^{10} eV reflects that of scattered-up photon around $E_\gamma \approx 10^5$ – 10^7 eV. When the energy of electron becomes ultra-relativistic, the oscillating structure is averaged out and vanishes.

Next, let us consider the photon case. When the energy of the incident photon is small ($E_\gamma < 10^3$ eV), the fractions of excitation and ionization are larger than that of heat. This is because the dominant energy loss mechanism is a photoelectron effect unless the ionization fraction is very close to unity. In this case, a photon ionizes an atomic hydrogen and emits a photoelectron whose energy is almost the same as the primary photon. Therefore, the behavior of photons is very similar to that of electrons at low energy. As photon energy increases, Compton scattering becomes the dominant energy loss. When the photon energy is larger than the electron mass, the forward scattering becomes dominant and the energy of the recoil electron approaches that of the photon. In other words, Compton scattering produces a recoil electron with the same energy as the incident photon. Therefore, the behavior of photons traces that of electrons in this energy region.

When photon energy is larger than 10^8 eV, the effects of pair production in matter, photon-photon scattering, and double photon pair creation cannot be neglected. However, it is hard to explain the influence of these processes because the most dominant process among the three depends on the redshift and photon energy, and the shape of the spectrum of secondary particles is very sensitive to primary photon energy. At high energy, however, the fractions of heat, excitation, and ionization become constant values just like the electron. As high energy photons are closely related with electrons, these constants will become almost the same value in either case.

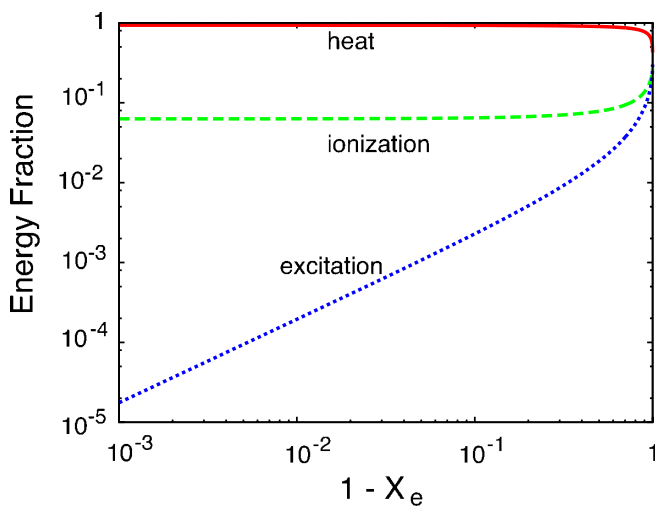


FIG. 11 (color online). Electron and photon energy degradation with $1 + z = 1000$. The solid line represents χ_h , the dashed line represents χ_i , and the dotted line represents χ_{ex} .

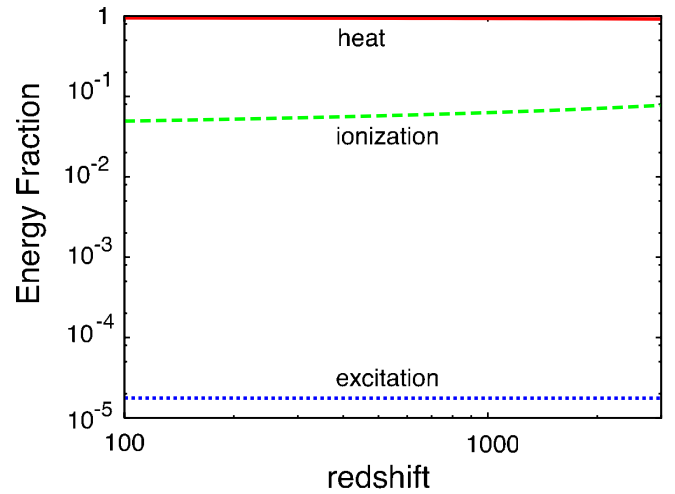


FIG. 12 (color online). Electron and photon energy degradation with $x_e = 10^{-3}$. The solid line represents χ_h , the dashed line represents χ_i , and the dotted line represents χ_{ex} .

To see how ionization fraction x_e and redshift z have influence on the energy degradation, we plot the fractions of heat, ionization, and excitation as a function of $1 - x_e$ and $1 + z$ in Figs. 11 and 12, respectively. Here we have taken 10^{12} eV for the initial energy of electrons or photons. This is because all of the fractions become constant values at this energy. Unless the ionization fraction is very small, χ_h and χ_i are almost independent of it. This is because χ_i is mainly determined by photoionization due to low energy secondary photons in this case and the collision frequency of photoionization is much larger than that of Compton scattering at low energy [Fig. 6]. Therefore the effect of the change of ionization fraction is almost irrelevant. However, the fraction of excitation χ_e is very sensitive to the ionization fraction since the collision frequency of electron impact excitation is in proportion to $1 - x_e$ while the competing processes (inverse Compton and Coulomb loss) are independent of $1 - x_e$. The fraction of heat χ_h does not depend on $1 - x_e$ since χ_i is independent of $1 - x_e$ and χ_{ex} is a very small quantity. (Please notice that $\chi_i + \chi_{ex} + \chi_h = 1$.) When the ionization fraction is very small, the effect of Coulomb scattering is weakened, and these fractions become the same order. Unlike the ionization fraction, the change of redshift seems to have no influence on the energy degradation. This is because the change of redshift affects which process is dominant at high energy but is almost irrelevant at low energy. χ_i and χ_e are determined by secondary low energy particles, and these fractions are nearly independent of the redshift.

V. CONCLUSIONS

We have carried out detailed calculations of the fractions of the initial energy of the injected electron or photon which are used to heat, ionize, and excite background plasma in the early Universe. In the high energy limit

($E > 10^{11}$ eV = 100 GeV), we have shown that the fractions are almost independent of the initial energy. In the energy range between 10 keV and 10 MeV, the fractions are sensitive to the initial energy, which shows that the simple extrapolation of the previous result is not appropriate.

Our calculations are valid up to TeV and can be applied to various cosmological and astrophysical situations. Once we know the fractions of ionization and heat, it is easy to estimate the ionization and heating rates caused by high energy photons (electrons) [see Eqs. (2)–(4)], and then we obtain the evolutions of ionization and electron temperature. As mentioned in the introduction, one of most interesting applications is to study the effect of TeV mass dark matter decay/annihilation on CMB angular spectra. We will investigate this subject in a separate paper.

ACKNOWLEDGMENTS

This work was supported in part by the Grant-in-Aid for Scientific Research from the Ministry of Education, Science, Sports, and Culture of Japan, No. 14102004 (M.K.). This work was supported by World Premier International Research Center Initiative (WPI Initiative), MEXT, Japan. This work was also supported in part by JSPS-AF Japan-Finland Bilateral Core Program.

APPENDIX: RELEVANT CROSS SECTIONS

In this appendix, we show the cross sections and energy loss rates adopted in this paper.

1. Electron

a. Excitation of H.—We have adopted almost the same cross sections for atomic hydrogen and Coulomb losses as Ref. [4]. For the cross sections for the electron impact excitation of atomic hydrogen, we have adopted Ref. [11]. At high energy, we have used the Bethe approximation reviewed in Refs. [12–15].

$$\sigma_{2p}(\text{NR}) = \frac{4\pi a_0^2}{T/\text{Ry}} \left[M_{2p}^2 \ln\left(\frac{4C_{2p}T}{\text{Ry}}\right) + \frac{\gamma_{2p}}{T/\text{Ry}} \right], \quad (\text{A1})$$

$$\sigma_{2p}(\text{R}) = \frac{8\pi a_0^2}{mv^2/\text{Ry}} M_{2p}^2 \left[\ln\left(\frac{\beta^2}{1-\beta^2}\right) - \beta^2 + \ln C_{2p} + 11.2268 \right], \quad (\text{A2})$$

where a_0 is the Bohr radius, Ry is the Rydberg energy, and $T = mv^2/2$ represents the kinetic energy. The numerical coefficients are $\ln C_{2p} = -0.89704$, $\gamma_{2p} = 0.207985$, and $M_{2p}^2 = 0.55493$. “NR” and “R” mean nonrelativistic and relativistic, respectively.

$$\sigma_{2s}(\text{NR}) = \frac{4\pi a_0^2}{T/\text{Ry}} \left[b_{2s} + \frac{\gamma_{2s}}{T/\text{Ry}} \right], \quad (\text{A3})$$

$$\sigma_{2s}(\text{R}) = \frac{8\pi a_0^2}{mv^2/\text{Ry}} b_{2s}, \quad (\text{A4})$$

where $b_{2s} = 0.11986$ and $\gamma_{2s} = -0.3125$.

$$\sigma_{n=3}(\text{NR}) = \frac{4\pi a_0^2}{T/\text{Ry}} \left[M_3^2 \ln\left(\frac{4C_3T}{\text{Ry}}\right) \right], \quad (\text{A5})$$

$$\sigma_{n=3}(\text{R}) = \frac{8\pi a_0^2}{mv^2/\text{Ry}} M_3^2 \left[\ln\left(\frac{\beta^2}{1-\beta^2}\right) - \beta^2 + \ln C_3 + 11.2268 \right], \quad (\text{A6})$$

where $M_3^2 = 8.8989 \times 10^{-2}$ and $\ln C_3 = -0.2724$.

For the excitation to $n > 3$, we subtract Eqs. (A1)–(A6) from the total excitation cross section.

$$\sigma_{\text{ex}}(\text{NR}) = \frac{4\pi a_0^2}{T/\text{Ry}} \left[M_{\text{ex}}^2 \ln\left(\frac{4C_{\text{ex}}T}{\text{Ry}}\right) + \frac{\gamma_{\text{ex}}}{T/\text{Ry}} \right], \quad (\text{A7})$$

$$\sigma_{\text{ex}}(\text{R}) = \frac{8\pi a_0^2}{mv^2/\text{Ry}} M_{\text{ex}}^2 \left[\ln\left(\frac{\beta^2}{1-\beta^2}\right) - \beta^2 + \ln C_{\text{ex}} + 11.2268 \right], \quad (\text{A8})$$

where $\ln C_{\text{ex}} = -0.5780$, $\gamma_{\text{ex}} = -0.120575$, and $M_{\text{ex}}^2 = 0.7166$.

b. Ionization of H.—For the ionization cross section, we have adopted the following differential cross section:

$$\frac{d\sigma_i(E, \epsilon)}{d\epsilon} = \frac{A(E)}{1 + (\epsilon/\bar{\epsilon})^2} \quad \text{for } 0 \leq \epsilon \leq \frac{1}{2}(E - I), \quad (\text{A9})$$

where E is the incident electron energy and ϵ is the energy of the ejected electron. We choose $\bar{\epsilon} = 8$ eV. In Eq. (A9), a value of 2 is different from that of 2.1 originally suggested by [16]. This is why Eq. (A9) can be analytically integrated. Two parameters $A(E)$ and $\bar{\epsilon}$ are related to the total ionization cross section $\sigma_i(E)$:

$$A(E) = \frac{\sigma_i(E)}{\bar{\epsilon}} [\tan^{-1} X(E)]^{-1}, \quad (\text{A10})$$

$$X(E) = \frac{E - I}{2\bar{\epsilon}}, \quad (\text{A11})$$

where I is the ionization potential. The total ionization cross section for atomic hydrogen had been measured by Ref. [17] in the range 14.6–4000 eV. Above 4000 eV, we used Bethe approximation [12,14].

$$\sigma_i(\text{NR}) = \frac{4\pi a_0^2}{T/\text{Ry}} \left[M_i^2 \ln\left(\frac{4C_iT}{\text{Ry}}\right) + \frac{\gamma_i}{T/\text{Ry}} \right], \quad (\text{A12})$$

$$\sigma_i(\text{R}) = \frac{8\pi a_0^2}{mv^2/\text{Ry}} M_i^2 \left[\ln\left(\frac{\beta^2}{1-\beta^2}\right) - \beta^2 + \ln C_i + 11.2268 \right], \quad (\text{A13})$$

where $M_i^2 = 0.2834$, $\ln C_i = 3.048$, and $\gamma_i = -1.6294 + \ln(\text{Ry}/T)$.

c. e^- -H collision.—For electron-hydrogen momentum transfer cross sections at low energies, we have adopted the results of [18,19]. The momentum loss cross section is described by

$$\sigma_{\text{mt}} = \frac{\pi a_0^2}{T/\text{Ry}} \sum_{l=0} [3\sin^2(\eta_{l+1}^- - \eta_l^-) + \sin^2(\eta_{l+1}^+ - \eta_l^+)], \quad (\text{A14})$$

where η_l^+ and η_l^- are the phase shift computed in [20,21]. The cross sections at 100, 200, and 300 eV were calculated in [22]. Cross sections at other energies were derived by interpolation and extrapolation. The energy loss due to electron-hydrogen momentum transfer is described by

$$\left[\frac{-dE}{dt} \right]_{\text{mt}} = \frac{2m_e E}{m_p} n_H v_e \sigma_{\text{mt}}(E), \quad (\text{A15})$$

where m_p is the proton mass.

d. Coulomb collision.—Incident electrons lose their energies due to elastic collisions with background electrons and photons. Energy loss is dominated by electrons at low energy since Coulomb cross sections are much larger than Compton cross sections. However, energy loss is dominated by photons at high energy since the number density of photons is much larger than that of electrons.

For the energy loss due to Coulomb collisions with background electrons, we have adopted the following analytical formula [23]:

$$\left[\frac{-dE}{dt} \right]_{\text{Cl}} = \frac{2.0 \times 10^{-4} n_e^{0.97}}{E^{0.44}} \left(\frac{E - E_e}{E - 0.53E_e} \right)^{2.36} \text{ eV s}^{-1}, \quad (\text{A16})$$

where E is the incident electron energy in eV, E_e is the background electron energy in eV, and n_e is the electron number density in cm^{-3} .

e. Inverse Compton scattering.—An important quantity which characterizes the behavior of inverse Compton scattering is γE_{CMB} (photon energy in the electron's rest frame), where E_{CMB} is the energy of the CMB photon. If γE_{CMB} is much less than m_e , a Thomson scattering approximation is valid. Otherwise, a Klein-Nishina cross section should be used.

For inverse Compton scattering with $\gamma E_{\text{CMB}} \ll m_e$, the energy spectrum of scattered photon is obtained by Ref. [8] in the limit $\beta \rightarrow 1$. However, we should keep β so as not to spoil the validity of the Thomson approximation. After some tedious calculations, the number of collisions per unit time and unit scattered photon energy (E_γ) is given by

$$\frac{d^2 N}{dt dx} = \sigma_T c n(E_{\text{CMB}}) dE_{\text{CMB}} f(x), \quad (\text{A17})$$

where σ_T is the Thomson cross section and $n(E_{\text{CMB}})$ is the differential number density of CMB photons and $x = E_\gamma/E_{\text{CMB}}$. The expressions for $f(x)$ is given by

$$f(x) = \frac{3}{16\gamma^4 \beta^4} \left[-(1 + \beta^2) \left(\frac{1}{1 + \beta} - \frac{x}{1 - \beta} \right) + (x^2(1 + \beta) - x(1 - \beta)) - 2x \ln \left(x \frac{1 + \beta}{1 - \beta} \right) \right] \quad (\text{A18})$$

for $\frac{1 - \beta}{1 + \beta} \leq x \leq 1$,

$$f(x) = \frac{3}{16\gamma^4 \beta^4} \left[-(1 + \beta^2) \left(\frac{x}{1 + \beta} - \frac{1}{1 - \beta} \right) + (x(1 + \beta) - x^2(1 - \beta)) - 2x \ln \left(\frac{1 + \beta}{x(1 - \beta)} \right) \right] \quad (\text{A19})$$

for $1 \leq x \leq \frac{1 + \beta}{1 - \beta}$.

The coefficient is determined so that $\int f(x) dx$ is equal to unity. In the limit $\beta \rightarrow 1$, Eq. (A19) corresponds to the result of [8]. The number of collisions per unit time and the energy loss rate can be easily obtained:

$$\int \frac{d^2 N}{dt dx} dx = \sigma_T c n(E_{\text{CMB}}) dE_{\text{CMB}} = \sigma_T c n_{\text{CMB}}, \quad (\text{A20})$$

$$\int \frac{d^2 N}{dt dx} (E_\gamma - E_{\text{CMB}}) dx = \frac{4}{3} \sigma_T c n(E_{\text{CMB}}) E_{\text{CMB}} dE_{\text{CMB}} \gamma^2 \beta^2 = \frac{4}{3} \sigma_T c U_{\text{CMB}} \gamma^2 \beta^2, \quad (\text{A21})$$

where n_{CMB} and U_{CMB} are the number and energy density of CMB photons, respectively.

For inverse Compton scattering with $\gamma E_{\text{CMB}} \geq m_e$, we should use a Klein-Nishina cross section instead of a Thomson cross section. The number of collisions per unit time and unit scattered photon energy is given by [24]

$$\frac{d^2 N}{dt d\alpha'} = \frac{2\pi r_e^2 c}{\alpha \gamma^2} \left[2q \ln q + (1 + 2q)(1 - q) + \frac{1}{2} \frac{(4\alpha \gamma q)^2}{1 + 4\alpha \gamma q} (1 - q) \right] n(E_{\text{CMB}}) dE_{\text{CMB}} \quad (\text{A22})$$

for $\alpha \leq \alpha' \leq \frac{4\alpha \gamma^2}{1 + 4\alpha \gamma}$,

where $\alpha = E_{\text{CMB}}/m_e$, $\alpha' = E_\gamma/m_e$, and $q = \alpha'/4\alpha\gamma^2(1 - \alpha'/\gamma)$. The number of collisions per unit time can be obtained by integrating Eq. (A22). We shall assume that Eq. (A22) is valid for $0 < q < 1$, even though Eq. (A22) is quite invalid for $0 < q < 1/4\gamma^2$. The contribution from the region $0 < q < 1/4\gamma^2$ is $O(1/\gamma^2)$ and is negligible since E_{CMB} is much less than m_e [24]. The

number of collisions per unit time is given by [25]

$$\int \frac{d^2 N}{dt d\alpha'} d\alpha' \simeq \int_0^1 \frac{d^2 N}{dt dq} dq = \sigma_T c \psi_1(s) n(E_{\text{CMB}}) dE_{\text{CMB}}, \quad (\text{A23})$$

where

$$\psi_1(s) = \frac{3}{2s^2} \left[\left(s + 9 + \frac{8}{s} \right) \ln(1+s) - 8 - \frac{2s+s^2}{2+2s} + 4\text{Li}_2(-s) \right], \quad (\text{A24})$$

and $s = 4\alpha\gamma$. The function $\text{Li}_2(x)$ is the dilogarithm

$$\text{Li}_2(x) \equiv - \int_0^x dz \frac{\ln(1-z)}{z}. \quad (\text{A25})$$

The energy loss rate is given by [24]

$$\int E_\gamma \frac{d^2 N}{dt d\alpha'} d\alpha' \simeq \frac{4}{3} \sigma_T c \gamma^2 \psi_2(s) n(E_{\text{CMB}}) E_{\text{CMB}} dE_{\text{CMB}}, \quad (\text{A26})$$

where

$$\psi_2(s) = \frac{9}{s^3} \left[\left(\frac{s}{2} + 6 + \frac{6}{s} \right) \ln(1+s) - \frac{6+13s+8s^2+11s^3/12}{(1+s)^2} + 2\text{Li}_2(-s) \right]. \quad (\text{A27})$$

2. Photon

a. Photoionization.—The absorption of x rays and γ rays is studied in detail in [26]. Incident photons are mainly absorbed by hydrogen atoms and eject photoelectrons at low energies. The photoionization cross section for atomic hydrogen was reviewed in [27,28].

$$\sigma_K(\text{NR}) = \frac{64\pi\sigma_T}{\alpha^3} \left(\frac{I}{h\nu} \right)^4 \frac{\exp(-4\eta\cot^{-1}\eta)}{1 - \exp(-2\pi\eta)}, \quad (\text{A28})$$

$$\sigma_K(\text{R}) = \frac{3\sigma_T\alpha^4}{4} \left(\frac{m_e}{h\nu} \right)^5 [\gamma^2 - 1]^{3/2} \left[\frac{4}{3} + \frac{\gamma(\gamma-2)}{\gamma+1} \times \left(1 - \frac{1}{2\gamma\sqrt{\gamma^2-1}} \ln \left(\frac{\gamma + \sqrt{\gamma^2-1}}{\gamma - \sqrt{\gamma^2-1}} \right) \right) \right], \quad (\text{A29})$$

where $h\nu$ is the incident photon energy, α is the fine-structure constant, I is the ionization energy, $\eta = 1/\sqrt{h\nu/I-1}$, and $\gamma = (h\nu + m_e)/m_e$. The cross sections above are just halves of [27,28]. This is because there is only one electron in the K shell in the case of hydrogen.

b. Compton scattering.—Incident photons interact with background electrons through Compton scattering. If photon energy is sufficient small, the energy of recoil electron is below the threshold energy of excitation and ionization

of atomic hydrogen. Therefore the energy transferred to the recoil electron can be regarded as heating. Besides, a photon loses only a small fraction of its energy per scattering. The energy loss due to Compton scattering is described by [26]

$$\left[\frac{-dE}{dt} \right]_{\text{Compton}} = m_e n_e c \sigma_T x^2 g(x), \quad (\text{A30})$$

where $x = h\nu/m_e$ and

$$g(x) = \frac{3}{8} \left[\frac{(x-3)(x+1)}{x^4} \ln(1+2x) + \frac{2(3+17x+31x^2+17x^3-\frac{10}{3}x^4)}{x^3(1+2x)^3} \right] \quad (\text{A31})$$

$$\simeq 1 \quad \text{for } x \ll 1 \quad (\text{A32})$$

$$\simeq \frac{3}{8x^2} \left(\ln 2x - \frac{5}{6} \right) \quad \text{for } x \gg 1. \quad (\text{A33})$$

If the photon energy is as large as the electron mass, a photon loses a sizable fraction of its energy per scattering. In this case, it is necessary to calculate the energy distribution of the recoil electrons. The cross section is given by the following Klein-Nishina formula:

$$\frac{d\sigma}{d\epsilon}(h\nu) = \frac{3\sigma_T}{8} \frac{m_e}{(h\nu)^2} \left[\frac{h\nu}{\epsilon} + \frac{\epsilon}{h\nu} + \left(\frac{m_e}{\epsilon} - \frac{m_e}{h\nu} \right)^2 - 2 \left(\frac{m_e}{\epsilon} - \frac{m_e}{h\nu} \right) \right] \quad (\text{A34})$$

for $\frac{m_e}{m_e + 2h\nu} h\nu \leq \epsilon \leq h\nu$,

where ϵ is the scattered photon energy.

c. Pair creation.—If the photon energy is larger than $2m_e$, it is possible to create an electron-positron pair. The energy and momentum conservation, however, are possible only if another particle is present. The differential cross section for pair creation in nuclei is given by the Bethe-Heitler formula [27,29]:

$$\frac{d\sigma}{dE_+} = \alpha r_e^2 \frac{p_+ p_-}{E_\gamma^2} \left\{ -\frac{4}{3} - 2E_+ E_- \frac{p_+^2 + p_-^2}{p_+^2 p_-^2} + m_e^2 \left(\frac{E_+ l_-}{p_-^3} + \frac{E_- l_+}{p_+^3} - \frac{l_+ l_-}{p_+ p_-} \right) + L \left[\frac{E_\gamma^2}{p_+^3 p_-^3} (E_+^2 E_-^2 + p_+^2 p_-^2) - \frac{8}{3} \frac{E_+ E_-}{p_+ p_-} - \frac{m_e^2 E_\gamma}{2p_+ p_-} \left(\frac{E_+ E_- - p_-^2}{p_-^3} l_- + \frac{E_+ E_- - p_+^2}{p_+^3} l_+ + \frac{2E_\gamma E_+ E_-}{p_+^2 p_-^2} \right) \right] \right\}, \quad (\text{A35})$$

where

$$p_{\pm} = \sqrt{E_{\pm}^2 - m_e^2}, \quad (\text{A36})$$

$$L = \ln \frac{E_+ E_- + p_+ p_- + m_e^2}{E_+ E_- - p_+ p_- + m_e^2}, \quad (\text{A37})$$

$$l_{\pm} = \ln \frac{E_{\pm} + p_{\pm}}{E_{\pm} - p_{\pm}}, \quad (\text{A38})$$

and E_{\pm} is the energy of the positron (electron). The analytical expression for the cross section is given by [29,30]

$$\begin{aligned} \sigma = \alpha r_e^2 \left\{ \frac{28}{9} \ln 2k - \frac{218}{27} + \left(\frac{2}{k}\right)^2 \left[6 \ln 2k - \frac{7}{2} \right. \right. \\ \left. \left. + \frac{2}{3} \ln^3 2k - \ln^2 2k - \frac{\pi^2}{3} \ln 2k + \frac{\pi^2}{6} + 2\zeta(3) \right] \right. \\ \left. - \left(\frac{2}{k}\right)^4 \left[\frac{3}{16} \ln 2k + \frac{1}{8} \right] \right. \\ \left. - \left(\frac{2}{k}\right)^6 \left[\frac{29}{9 \times 256} \ln 2k - \frac{77}{27 \times 512} \right] + \dots \right\} \\ \text{for } k > 4, \quad (\text{A39}) \end{aligned}$$

where $k = E_{\gamma}/m_e$. Convenient approximate formulas are given by Ref. [31] which are valid for $k \leq 20$:

$$\frac{d\sigma}{dx} = \alpha r_e^2 \phi_0 z [1 + 0.135(\phi_0 - 0.52)z(1 - z^2)], \quad (\text{A40})$$

where

$$x = \frac{E_+ - m_e}{E_{\gamma} - 2m_e}, \quad (\text{A41})$$

$$z = 2\sqrt{x(1-x)}, \quad (\text{A42})$$

and ϕ_0 is the differential cross section for equal partition of energy $E_+ = E_- = E_{\gamma}/2$. The second term in the square brackets should be dropped when it becomes negative (below $k = 4.2$). ϕ_0 is given by

$$\begin{aligned} \phi_0 = (1 - \gamma_1) \left[\frac{1}{3}(4 - \gamma_1^2)(L_1 - 1) - \gamma_1^2 \alpha_1 (\alpha_1 - 1) \right. \\ \left. - \gamma_1^4 \alpha_1 (L_1 - \alpha_1) \right], \quad (\text{A43}) \end{aligned}$$

where

$$\gamma_1 = \frac{2}{k}, \quad (\text{A44})$$

$$L_1 = \frac{2}{1 - \gamma_1^2} \ln \left(\frac{k}{2} \right), \quad (\text{A45})$$

$$\alpha_1 = \frac{1}{\sqrt{1 - \gamma_1^2}} \ln \left[\frac{k}{2} + \sqrt{\left(\frac{k}{2} \right)^2 - 1} \right]. \quad (\text{A46})$$

We get from Eq. (A40) for the total cross section

$$\sigma = \frac{\pi}{4} \alpha r_e^2 \phi_0 \quad \text{for } k < 4.2 \quad (\text{A47})$$

$$= \alpha r_e^2 (0.776 \phi_0 + 0.018 \phi_0^2) \quad \text{for } k > 4.2. \quad (\text{A48})$$

d. Photon-photon scattering.—If the photon energy is below the effective threshold energy of the double photon pair creation, the photon-photon scattering ($\gamma\gamma \rightarrow \gamma\gamma$) process becomes significant. The photon-photon scattering rate for $E_{\gamma} E_{\text{CMB}} \leq m_e^2$ is given by [32]

$$P(E_{\gamma}) = 3.33 \times 10^{11} \left(\frac{T_{\text{CMB}}}{m_e} \right)^6 \left(\frac{E_{\gamma}}{m_e} \right)^3 \text{ s}^{-1}. \quad (\text{A49})$$

The normalized distribution of secondary photons of energy E'_{γ} is given by

$$\begin{aligned} p(E'_{\gamma}, E_{\gamma}) = \frac{20}{7} \frac{1}{E_{\gamma}} \left[1 - \frac{E'_{\gamma}}{E_{\gamma}} + \left(\frac{E'_{\gamma}}{E_{\gamma}} \right)^2 \right]^2 \\ \text{for } 0 \leq E'_{\gamma} \leq E_{\gamma}. \quad (\text{A50}) \end{aligned}$$

The distribution $p(E'_{\gamma}, E_{\gamma})$ satisfies

$$\frac{1}{2} \int_0^{E_{\gamma}} p(E'_{\gamma}, E_{\gamma}) dE'_{\gamma} = 1, \quad (\text{A51})$$

$$\int_0^{E_{\gamma}} p(E'_{\gamma}, E_{\gamma}) E'_{\gamma} dE'_{\gamma} = E_{\gamma}. \quad (\text{A52})$$

The above formulas are not valid for a larger value of E_{γ} . However, photon-photon scattering is not significant for high energy photons since double photon pair creation is the dominant process. Therefore, instead of using exact formulas, we simply neglect photon-photon scattering for $E_{\gamma} E_{\text{CMB}} > m_e^2$.

e. Double photon pair creation.—For high energy photon, double photon pair creation ($\gamma\gamma \rightarrow e^+ e^-$) is the dominant process. The total cross section for double photon pair creation is given by [33]

$$\sigma = \frac{1}{2} \pi r_e^2 (1 - \beta^2) \left[(3 - \beta^4) \ln \frac{1 + \beta}{1 - \beta} - 2\beta(2 - \beta^2) \right], \quad (\text{A53})$$

where β is the electron (positron) velocity in the center-of-mass system. The relationship between β and E_{γ} , E_{CMB} , and θ which is the angle between the momenta of the colliding photons is easily obtained:

$$\beta = \sqrt{1 - \frac{1}{s}}, \quad (\text{A54})$$

$$s = \frac{E_{\gamma} E_{\text{CMB}}}{2m_e^2} (1 - \cos\theta). \quad (\text{A55})$$

Clearly, the threshold energy for double photon pair production is $E_{\gamma} = m_e^2/E_{\text{CMB}}$, head-on photon collision ($\theta = \pi$, $s = 1$). For calculation of the absorption probability, we

should average the above cross section over the distributions for isotropically distributed photons [25,33]:

$$\begin{aligned}\sigma_{\text{ave}} &= \frac{1}{2} \int_{-1}^{1-2m_e^2/E_\gamma E_{\text{CMB}}} (1 - \cos\theta) \sigma d \cos\theta \\ &= \frac{3}{8} \sigma_T \left(\frac{m_e^2}{E_\gamma E_{\text{CMB}}} \right)^2 \left[\frac{1 + 2v + 2v^2}{1 + v} \ln \omega \right. \\ &\quad \left. - 2\sqrt{\frac{v}{1+v}}(1 + 2v) + 2\ln^2(1 + \omega) - \ln^2 \omega \right. \\ &\quad \left. + 4\text{Li}_2\left(\frac{1}{1 + \omega}\right) - \frac{\pi^2}{3} \right],\end{aligned}\quad (\text{A56})$$

where

$$v = \frac{E_\gamma E_{\text{CMB}}}{m_e^2} - 1 > 0, \quad (\text{A57})$$

$$\omega = \frac{\sqrt{1+v} + \sqrt{v}}{\sqrt{1+v} - \sqrt{v}}. \quad (\text{A58})$$

Differential spectra of electrons and positrons are given by [34]

$$\begin{aligned}\frac{d\sigma}{dE_e} &= \frac{\pi r_e^2 m_e^4}{4E_\gamma^3 E_{\text{CMB}}^2} \left[\frac{4E^2}{E_e E_p} \ln \frac{4E_{\text{CMB}} E_e E_p}{m_e^2 E} - \frac{8E_{\text{CMB}} E}{m_e^2} \right. \\ &\quad \left. + \frac{2(2E_{\text{CMB}} E - m_e^2) E^2}{m_e^2 E_e E_p} - \left(1 - \frac{m_e^2}{E_{\text{CMB}} E} \right) \frac{E^4}{E_e^2 E_p^2} \right],\end{aligned}\quad (\text{A59})$$

where E_e (E_p) is the energy of the electron (positron) and E is the total energy, $E = E_e + E_p = E_\gamma + E_{\text{CMB}}$. The limits of the variation of E_e (E_p) are given by

$$\frac{E}{2} \left(1 - \sqrt{1 - \frac{m_e^2}{E_{\text{CMB}} E}} \right) \leq E_e \leq \frac{E}{2} \left(1 + \sqrt{1 - \frac{m_e^2}{E_{\text{CMB}} E}} \right). \quad (\text{A60})$$

3. Positronium

Here we show the energy spectrum from three-photon annihilation of positronium. The energy spectrum is continuous, as allowed by conservation of momentum. It has been calculated in Ref. [35] with photon energy η normalized by the electron mass:

$$\begin{aligned}F(\eta) &= \frac{2}{\pi^2 - 9} \left[\frac{\eta(1-\eta)}{(2-\eta)^2} - \frac{2(1-\eta)^2}{(2-\eta)^3} \ln(1-\eta) \right. \\ &\quad \left. + \frac{2-\eta}{\eta} + \frac{2(1-\eta)}{\eta^2} \ln(1-\eta) \right], \quad \text{for } 0 \leq \eta \leq 1\end{aligned}\quad (\text{A61})$$

The function $F(\eta)$ is normalized so that

$$\int_0^1 d\eta F(\eta) = 1. \quad (\text{A62})$$

-
- [1] D.N. Spergel *et al.*, *Astrophys. J. Suppl. Ser.* **170**, 377 (2007).
[2] M. Kawasaki, K. Kohri, and T. Moroi, *Phys. Lett. B* **625**, 7 (2005); *Phys. Rev. D* **71**, 083502 (2005).
[3] W. Hu and J. Silk, *Phys. Rev. Lett.* **70**, 2661 (1993).
[4] A. Dalgarno, M. Yan, and W. Liu, *Astrophys. J. Suppl. Ser.* **125**, 237 (1999).
[5] X. Chen and M. Kamionkowski, *Phys. Rev. D* **70**, 043502 (2004).
[6] N. Padmanabhan and D.P. Finkbeiner, *Phys. Rev. D* **72**, 023508 (2005).
[7] V.L. Ginzburg and S.I. Syrovatskii, *The Origin of Cosmic Rays* (Pergamon Press, New York, 1964).
[8] G.R. Blumenthal and R.J. Gould, *Rev. Mod. Phys.* **42**, 237 (1970).
[9] A. Dalgarno and G. Lejeune, *Planet. Space Sci.* **19**, 1653 (1971).
[10] C.J. Crannell, G. Joyce, R. Ramaty, and C. Werntz, *Astrophys. J.* **210**, 582 (1976).
[11] I. Shimamura, *Sci. Pap. Inst. Phys. Chem. Res.* **82**, 1 (1989).
[12] M. Inokuti, *Rev. Mod. Phys.* **43**, 297 (1971).
[13] M. Inokuti, Y. Itikawa, and J.E. Turner, *Rev. Mod. Phys.* **50**, 23 (1978).
[14] Y.-K. Kim and M. Inokuti, *Phys. Rev. A* **3**, 665 (1971).
[15] M. Inokuti, Argonne National Laboratory Report No. ANL-6769, 1963, p. 7.
[16] C.B. Opal, W.K. Peterson, and E.C. Beaty, *J. Chem. Phys.* **55**, 4100 (1971).
[17] M.B. Shah, D.S. Elliott, and H.B. Gilbody, *J. Phys. B* **20**, 3501 (1987).
[18] B.H. Bransden, A. Dalgarno, T.L. John, and M.J. Seaton, *Proc. Phys. Soc. London* **71**, 877 (1958).
[19] A. Dalgarno and G.W. Griffing, *Proc. R. Soc. A* **248**, 415 (1958).
[20] M.R.H. Rudge, *J. Phys. B* **8**, 940 (1975).
[21] J.N. Das and M.R.H. Rudge, *J. Phys. B* **9**, L131 (1976).
[22] W.L. van Wyngaarden and H.R.J. Walters, *J. Phys. B* **19**, 929 (1986).
[23] W.E. Swartz, J.S. Nisbet, and A.E.S. Green, *J. Geophys. Res.* **76**, 8425 (1971).
[24] F.C. Jones, *Phys. Rev.* **167**, 1159 (1968).
[25] A.A. Zdziarski, *Astrophys. J.* **335**, 786 (1988).
[26] A.A. Zdziarski and R. Svensson, *Astrophys. J.* **344**, 551 (1989).

- [27] W. Heitler, *The Quantum Theory of Radiation* (Oxford University Press, London, 1954), 3rd ed.
- [28] K. R. Lang, *Astrophysical Formulae* (Springer, Berlin, 1999), 3rd ed.
- [29] J. W. Motz, H. A. Olsen, and H. W. Koch, *Rev. Mod. Phys.* **41**, 581 (1969).
- [30] L. C. Maximon, *J. Res. Natl. Bur. Stand. Sect. B* **72**, 79 (1968).
- [31] P. V. C. Hough, *Phys. Rev.* **73**, 266 (1948).
- [32] R. Svensson and A. A. Zdziarski, *Astrophys. J.* **349**, 415 (1990).
- [33] R. J. Gould and G. P. Schreder, *Phys. Rev.* **155**, 1404 (1967).
- [34] F. A. Agaronyan, A. M. Atyan, and A. N. Najapetyan, *Astrophysics (Engl. Transl.)* **19**, 187 (1983).
- [35] A. Ore and J. L. Powell, *Phys. Rev.* **75**, 1696 (1949).